Insights from MD Simulation on Na^+ Binding and Loop Dynamics in Multidrug Resistance Transporter Norm

Jun Du[1], GuanFu Duan[1], Changge Ji[1,2], Jianing Song[2*], and John Z.H. Zhang[1,2,3*]

[1]*Shanghai Engineering Research Center for Molecular Therapeutics and New Drug Development, Shanghai Key Laboratory of Green Chemistry and Chemical Processes, School of Chemistry and Molecular Engineering, East China Normal University, Shanghai 200062, China*

[2]*NYU-ECNU Center for Computational Chemistry, NYU Shanghai, Shanghai 200062, China*

[3]*Department of Chemistry, New York University, NY, NY 10003, USA*

*Correspondence to: js8884@nyu.edu, john.zhang@nyu.edu,

Abstract:

The multidrug resistance transporter NorM is an important drug resistance pump and plays a critical role in multidrug resistance in bacteria and mammals. In this study we carried out molecular dynamics simulation to study the mechanism of Na^+ binding and dynamical structures of two long loops in the substrate-releasing process in substrate binding NorM. Our simulation study identified several key residues (D41, E261 D377) along the Na^+ binding pathway and a multi-state ion-binding mechanism is proposed based on the simulation study. In this proposed model, the transport of Na^+ is a multi-stage process with D41 being the first station for binding to Na^+, followed by Na^+ binding to the second station E262 and finally to the cation-binding site of E262 and D377. During the transport of Na^+, the transmembrane components TM1, TM7 and TM2 are rearranged to facilitate the ion transport as well conformational changes of NorM to a closed state. Further, substrate-bound simulation revealed that Loop3-4 and Loop9-10 control the substrate-releasing process.

Key words: MDR transporters; MATE family; NorM; MD simulation; loops; sodium ions

Preprints (www.preprints.org) | NOT PEER-REVIEWED | Posted: 30 August 2018 doi:10.20944/preprints201808.0532.v1

Introduction

Multidrug resistance [1-3] presents an increasing threat to drug treatment of cancers and infectious diseases. The resistance is caused by multidrug transporters (membrane proteins) that can mediate the export of a broad range of chemically unrelated and structurally dissimilar xenobiotics and toxic metabolites from cells in both prokaryotes and eukaryotes[4]. Multidrug transporters are categorized into five sub-families[5, 6]: the ATP-binding cassette (ABC) family, the major facilitator superfamily (MFS), the resistance-nodulation-division (RND) family, the small multidrug resistance (SMR) family, and the multidrug and toxic compound extrusion (MATE) family. ABC transporters are membrane ATPases which couple drug extrusion with the hydrolysis of ATP[7], while MATE and other sub-families belong to secondary transporters that use an electrochemical gradient of H^+ or Na^+ ions to drive drugs across the membrane[4].

Various MATER family members were discovered over the past decade [8-10] and their important functions in humans are began to unravel [7, 11]. The first atomic structure of MATE family member NorM_VC (without ligand binding) was reported in 2010 [12, 13] and subsequently, the substrates-bound NorM transporter NorM_NG was published [14]. The NorM_NG structures are in the extracellular-facing, substrate-bound states. These structures revealed how a MATE transporter interacts with various cationic and poly-aromatic substrates for the first time, and made it possible to study the conformational changes of NorM protein upon substrate binding from a theoretical perspective at atomic detail. The complete structure of NorM_NG is composed of 12 trans-membrane helices. The N-domain (TM1-6) and C-domain (TM7-12) are connected by intervening loops and form a hydrophobic central cavity. In substrates-bound NorM_NG structures, the substrate-binding site is occupied by three different substrates (P4P, RHQ, ETT), which form complex close-range interactions between the residues of NorM_NG and the substrates.

A previous MD simulation study [15] on NorM_VC found an interesting two-Na^+ binding mode around the binding sites with residue E261 and D377. The newly published NorM_NG provides us new opportunity to study the dynamics of ions and proteins with substrate bounding. In this work, we performed molecular dynamics (MD) simulations to elucidate the dynamics of Na^+ binding and substrate transport in NorM. A total of nine-independent all-atom MD simulations have been performed in a lipid bilayer with or without sodium binding and in different solvation (NaCl or KCl) and in apo-/bound state of NorM_NG (simulation details are given in Table1). Further, aMD simulation is employed to study enhanced conformational changes of NorM in KCl solvent. Our result provids important insight on ions binding dynamics in different solvation and helps elucidate the dynamics and molecular mechanism underlying the drug extrusion process of NorM_NG.

Materials and methods:

System Setup

The initial structure for Apo-NorM_NG simulation comes from its crystal structure in

Preprints (www.preprints.org) | NOT PEER-REVIEWED | Posted: 30 August 2018 doi:10.20944/preprints201808.0532.v1

protein data bank (PDB code 4HUL[14] with Cs^+ directly removed). All the simulations with Na^+ ion bound are performed by directly inserting Na^+ into the protein at the same position of Cs^+ ion. The substrate-bound states of NorM_NG (P4P, RHQ, ETT[14]) are from the crystal structures with PDB ID 4HUK, 4HUN, 4HUM, respectively. CHARMM-GUI[16-20] is used to help build the bilayers system, with POPE lipids[21] and TIP3P[22] water used. A 0.1 mol/L counter-ions of NaCl or KCl are added to maintain the ion concentration in these simulations and to investigate the different effects of ion on protein dynamics. The final system contains about ~200 POPE molecules and ~13228 water molecules with the starting dimension 90 Å * 96 Å * 90 Å, about 84746 atoms in total with slightly different for each simulation system. The parameters for three different substrates are built from antechamber as follows. Firstly, the structure of each substrate is optimized at HF/6-31G* level, and then its atomic charges are fitted through RESP[23] at MP2/6-31G* level. The quantum chemical calculations are performed by Gaussian. Finally, GAFF[24] force field is used to generate the force filed parameters for these substrates used in simulations.

MD simulations

All MD simulations are performed using pmemd.cuda in AMBER12[25-27] with amber12 force field for protein, and GAFF force field for substrates. The particle mesh Ewald (PME)[28, 29] is used to treat the long-range electrostatic interactions. A cutoff of 12 Å is applied to treat van der Waals interactions. Periodic boundary condition (PBC) is imposed on all directions. Time-step is 2fs with SHAKE[30] used to constrain all the hydrogen atoms. Langevin dynamics[31] is applied to control the temperature, with a collision frequency of 1.0 ps^{-1}. Berendsen' weak coupling is used to control the pressure. First, the system is minimized with protein and the head of the lipids constrained for 10ps. Then protein and the head of lipids continue to be constrained for 270ps with the force constant gradual changes from 10kal/mol (protein)/2.5kcal/mol (lipids) to 0.5kcal/mol (protein)/0.1kcal/mol (lipids). The protein is constrained for another 100ps with force constant 0.1kcal/mol and the lipids are set free now. Thirdly, the whole systems are released for a 10 ns equilibration in an NPT ensemble. Finally, the systems are subjected to cMD simulation for 800 ns and a 350ns aMD simulation[21, 32-41] (only for Apo-NorM_NG in KCl) at constant temperature 310K. The aMD protocol modifies the initial potential energy surface of biomolecules, by adding a non-negative bias potential, and allows the system sample the conformational space more efficiently. E and α are two important parameters in aMD simulations. In this work, the value E and α come from the following equation suggested by J. A. McCammon in the membrane protein simulation job[41]: $E = V_{av} + V_{av}*c$, where V_{av} is the average dihedral energy from 10 ns cMD simulation and c is a constant and should be specified by the user. Here, the constant c is chosen as 0.4 from our previous experience. Thus $E_{0.4} = V_{av} + V_{av}*0.4$ and $\alpha = E_{0.4}/5$ is used to conduct the aMD simulation. The initial states and simulation details for the nine-independent all-atoms simulations are summarized in Table1.

Preprints (www.preprints.org) | NOT PEER-REVIEWED | Posted: 30 August 2018 doi:10.20944/preprints201808.0532.v1

Table1 Summary of the initial states and simulation lengths for the nine all-atom simulations.

Bio-system	Initial MD state		Simulation Length (ns)/Name		
	Solvation	Ligand/ions	cMD	aMD	Name
4HUL	NaCl	/	810	/	cMD1
	KCl	/	810	350	cMD2/aMD1
	NaCl	Na	810	/	cMD3
	KCl	Na	810	/	cMD4
4HUK	KCl	P4P	810	/	cMD5
	NaCl	P4P	810	/	cMD6
4HUN	NaCl	RHQ	810	/	cMD7
4HUM	NaCl	ETT	810	/	cMD8

Results and Discussions

Key residues and TMs rearrangements verified along the ions binding pathway

NorM can harness the Na^+ electrochemical gradient to export structurally and chemically distinct therapeutic drugs across cell membranes. As known, the substrate binding pockets are different from the ions-binding pockets. The central cavity binds the substrate, which can be confirmed from the crystal structures provided in *Methods* section. The ion binding pocket is not confirmed by crystals due to the replacement of Na^+ with Cs^+ in the experiments in order to make the positions of ions more easily determined when crystalized. But, the ion binding pocket could be quite well defined around residues E261 and D377 either by theoretical studies [42, 43] or other experimental structures related or close to the NorM family. However, question

Preprints (www.preprints.org) | NOT PEER-REVIEWED | Posted: 30 August 2018 doi:10.20944/preprints201808.0532.v1

of how the Na^+ enter into its binding pocket and the dynamics of Na^+ around its entering pathway is still largely unknown. Here, we compare the dynamics of NorM in different solvation NaCl or KCl in its apo-state or Na^+-bound state, to expect to shed some lights on these interesting and uncovered questions.

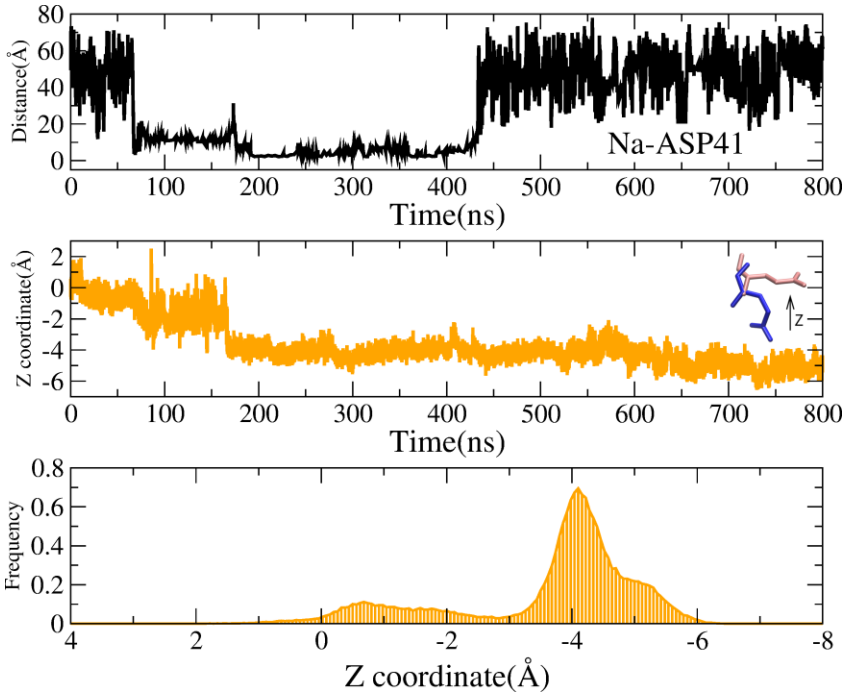

Figure 1 The dynamics of Na^+ and E261 in Apo-NorM simulation in solvent NaCl. Top panel: the changes of distance between the entering Na^+ ion and D41 as a function of time. Middle panel: the changes of Z coordinate of COO^- of E261 as a function of time. Pink color: the directions of COO^- in XRD structure, bule color: the direction of COO^- in the final MD structure. Bottom panel: The distributions of Z coordinates of COO^- of E261 during 800 ns simulation.

Figure 1 shows the dynamics of Na^+ and the group of COO^- of E261 in Apo-NorM simulation in solvation NaCl (corresponding cMD1 simulation in Table 1). The top panel of Figure 1 shows the changes of the distance between one Na^+ ion and D41 as a function of simulation time. It is seen that a sodium ion enters into the channel of NorM at about 60ns, and begins to tightly interact with D41 at around 175ns with a distance of 3.0 Å. After stays around and interacts with D41 for a long 250ns simulation length, the entered Na^+ ion finally leaves the channel at around 425ns and diffuses into the solvation and never comes back during the rest of 350ns simulation time. As has been stated, the binding pocket of Na^+ is around E261 and D377 in the middle of the channel, so why Na^+ stays around D41 for such a long a time, but finally chooses to leave the channel.

To address this question, time evolution of the coordinate of the carboxylic groups of E261 (D377 has almost no changes, thus data not shown) and the corresponding histograms are plotted in Figure 1 (yellow color in middle panel and bottom panel). From the middle panel, it is seen that the direction of COO^- of E261 at around zero almost vertical to Z axis at the

Preprints (www.preprints.org) | NOT PEER-REVIEWED | Posted: 30 August 2018 doi:10.20944/preprints201808.0532.v1

beginning of the simulation (pink color in the structure picture), and gradually changes to -4 Å at around 175ns, the moment when the entered Na^+ ion begins to tightly interact with D41. Then during the following 400ns simulation, the group COO^- stays at this negative direction opposite to the position where locate the entered Na^+ ion and the amino acid are D41, and even finally reaches to -6 Å (blue color in the structure picture). This obvious change of directions of E261 is also been clearly shown in the bottom panel of the distributions of COO^- of E261. The group COO^- of E261 is initially at zero and changes and stays around -4 Å for most of simulation time.

The conformational changes of COO^- group of E261 illustrate the reason why the entered sodium ion finally leaves the binding pocket. The Na^+ ion is to be transported to the binding site and help change the conformations of NorM. But now, the bridge of the transport has been interrupted by the direction change of COO^- of E261. As known from the definition of the ensemble, lots of tasks happen time to time, the entering of sodium and reaching to its binding pocket happen when all the key residues are in the right position. That is, the reaching of binding site of Na^+ ion is synergistically related to the dynamics of D41 and E261. If one of the required preconditions is not satisfied, this ion binding process fails and the sodium ion has to wait for another chance to drift to its cation-binding pocket. Further, the simulation details from cMD1 clearly show D41 is probably the first station of sodium ions binding to its pocket.

To compare, solvation of KCl is added to see the effect of other ions like K^+ on the dynamics of the channel of Apo-NorM (cMD2 simulation in Table1). Figure 2 shows the changes of the distances between the two entered K^+ ions and D41/E261 as a function of time. From the top two panels of Figure 2, it is clearly observed that a potassium ion (Ion1) enters into the channel and interacts with D41 at around 120ns production run, then moves close to E261, and locates between these two residues with around a steady distance around 3 Å, and finally escapes from the channel at around 740ns. Another potassium ion (Ion2) approaches the D41 and E216 directly after 220ns and stays there with a distance around 3 Å during the rest of 580ns simulation length (the right two panels of Figure 2). It is seen that Ion2 enters into the channel after Ion1, and during 500ns simulation length, both of these two K^+ ions interact with D41 and E261. One snapshot of the two-K^+-binding mode is shown in Figure S1 (yellow balls). These two K^+ ions coordinate to each of the carboxylic groups of D41 and E261 and remain steady at almost equal distance during a long simulation time in cMD2. This binding mode is similar to the two-Na^+-binding-mode found in our previous study of NorM_VC. Ion1 leaves the channel may be due to the reason that NorM could not transport two ions at the same time. The reason for Ion2 remained in the bridge built by D41 and E261 may due to our limited simulation time. But importantly, it is concluded that the ion binding process needs the bridge built by D41 and E261. Another interesting phenomenon observed in cMD2 simulation is that two trans-membrane helices, TM1 and TM7, each of which contain D41 and E261, move close to each other (shown in Figure S2). This interesting fact shows the conformational changes of NorM upon the transfer of K^+ ions from D41 and E261.

Preprints (www.preprints.org) | NOT PEER-REVIEWED | Posted: 30 August 2018 doi:10.20944/preprints201808.0532.v1

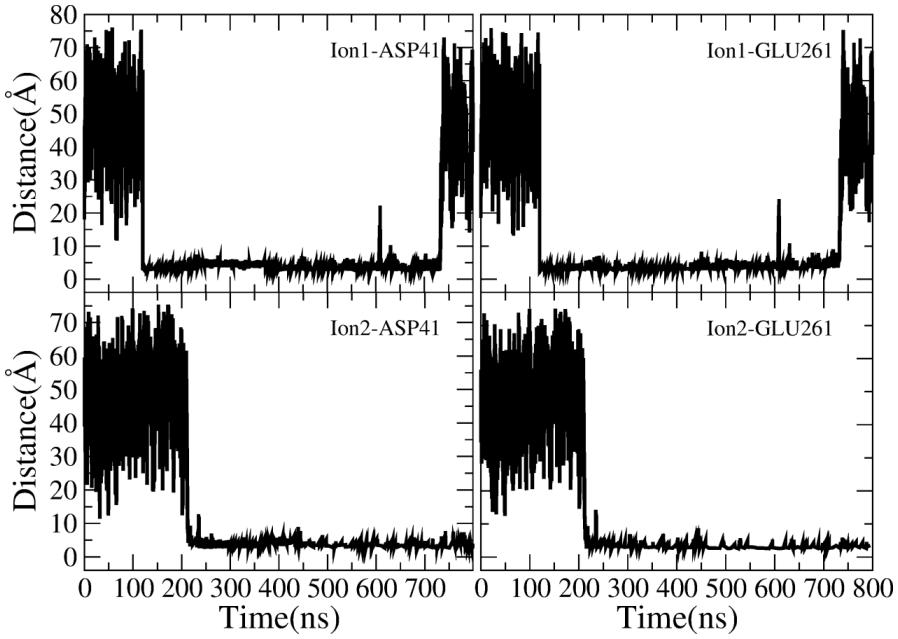

Figure 2 Time evolutions of the distance between the two entered K^+ ion and D41/E261.

The above analyses in cMD2 simulation clearly show D41 is the first station of the ions entering into the channel. Then a bridge between D41 and E261 is built to allow the ions to be transferred into the second station. The phenomenon of the missing transfer of ions in cMD1 is that the direction of E261 in cMD1 simulation is negatively parallel to Z-axis, leading to the failure of building the bridge between D41 and E261. The rearrangement of TM1 and TM7 is critical in this ion binding process.

D41 and E261 show different dynamics in different simulation environments. It is wondered the behaviors of these two residues upon Na^+ bound to NorM. Thus, we perform simulations with NorM bound by Na^+ in different solvation NaCl (cMD3 in Table1) and KCl (cMD4 in Table1). As been stated in *Methods,* Na^+ is directly inserted into NorM as the same position of Cs^+ ion.

The changes of the distance between the binding Na^+ ions and the carboxyl group (COO^-) of E261 and D377 remain stable near around 2.5Å, with only slight fluctuations (shown in Figure S3). There is no additional Na^+ ion in the solvation observed to enter into the channel of NorM. To investigate this interesting situation, the dynamics of D41 is examined and shown in Figure 3. It is seen that the direction of D41 turns from the right (towards the transport channel) in the XRD structure (pink color) to the left (opposite to the channel) in final snapshot of cMD3 simulation (blue color). The Y coordinate of the carboxyl group of D41 is -3.1Å in the crystal structure, while the value fluctuates from 0Å to 3Å in MD simulation, totally reversed in Y-axis. This reverse buries D41 in the region surrounded by TM1 and TM5. This dramatic conformational change of D41 disables D41 to coordinate Na^+ ion and eliminate its function as the first station along the pathway. Thus, it is reasonable no sodium ions can enter into the

Preprints (www.preprints.org) | NOT PEER-REVIEWED | Posted: 30 August 2018 doi:10.20944/preprints201808.0532.v1

channel with the destructive first station during their way to the binding site.

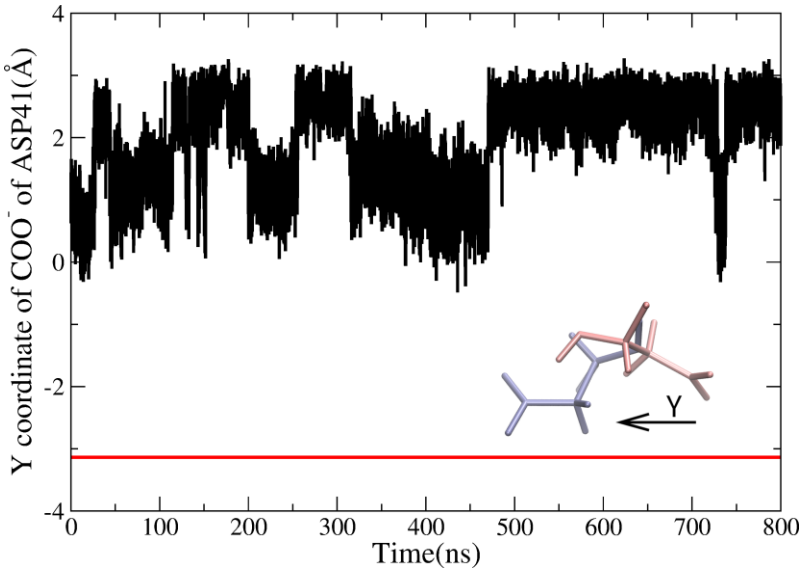

Figure 3 Time evolutions of the Y coordinates of COO^- group of D41 (black line). Red line: the Y coordinates of COO^- group of D41 in XRD structure. Pink color: the directions of COO^- in XRD structure, Light bule color: the direction of COO^- in the final MD structure.

In cMD3 simulation, sodium is bound in the binding site, while substrate is not bound in the central cavity, this state of NorM can be regarded as the state where NorM just release the substrate out of the cell with sodium entering the binding site, and prepares to perform conformational changes from outward-facing to inward-facing. Thus, the swing of D41 may help NorM to close the central cavity accessible from the outside of cell. To investigate this hypothesis, the final MD structure of NorM (light blue color) is superimposed to the initial XRD structure (pink color) to examine the dynamics of the TMs in NorM (shown in Figure 4). It is observed that TM2 in the final cMD3 simulated structure moves close to the TM1, TM7 and TM8. The conformation of NorM becomes more compact compared to that in the crystal structure. TM2 is like an obstacle block at the entrance to prevent the extracellular ions from drifting into the center cavity, and make the entire structure of NorM not accessible from the outside of cell. The conformational change of TM2 and the swing of D41 together make NorM a relatively occlude state, which is a quite important state during the transport cycle in Multidrug family.

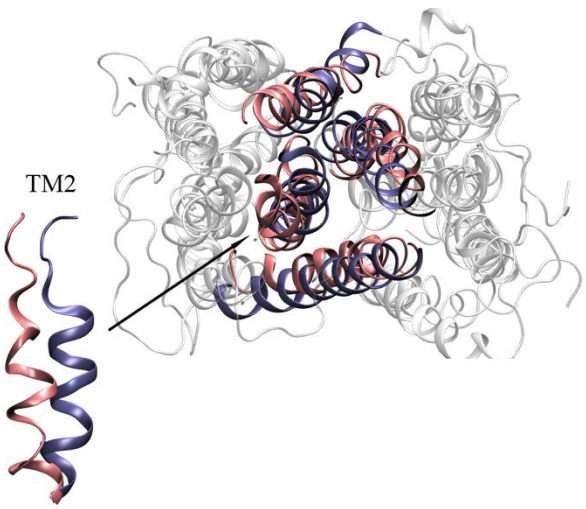

 doi:10.20944/preprints201808.0532.v1

Figure 4 The final MD structure (light blue color) of NorM in cMD3 is superimposed to the initial XRD structure (pink color), with TM2 enlarged in the bottom left of this figure.

The situation is quite different when it comes to the simulation of Na^+-bound-NorM in KCl solution (cMD4 simulation in Table 1). Figure 5a shows the changes of Z coordinates of bound Na^+ as a function of time. It is seen that this Na^+ ion goes up along the channel from zero Å to high to 8 Å, where D41 locates. Figure 5b shows time evolutions of the distances between this Na^+ and D41/E261/D377, respectively. Both of the distances between the Na^+ ion and the carboxyl group (COO^-) of E261 and D377 rise to ~15 Å during the rest of the 220 simulation time. The Na^+ ion leaves its binding site (middle/bottom panel in Figure 5b) and climbs up along the channel to site D41 (top panel in Figure 5b) and coordinates with it. The only difference between cMD3 and cMD4 simulation is the solvation used. Thus, the dynamics of K^+ ions are investigated.

Figure 6 describes the time evolutions of the Z coordinates of the entered K^+ ions into the channel in cMD4 simulation. Each color represents one K^+ ion entering into the channel. There are seven K^+ ions in total drifting into the channel and staying for different simulation time length, and only one finally stays in the binding site (red color). Figure 5 and Figure 6 clearly witness a process of Na^+-K^+ ion exchanges. As known, K^+ has a similar radius and a similar volume with Na^+, the transfer and binding of K^+ ions in NorM along the channel probably can be analogized to Na^+ ions. From this perspective, cMD4 simulation shows a picture of Na^+ ions released from the binding pocket before NorM closes itself to an occluded state. This is reasonable to consider that sodium ions should be able to freely access the channel before the central cavity closes, with the necessary preconditions of the right directions of D41 and E261. In cMD3 with NaCl solution, the inversing direction of D41 in Y-axis makes the entering of sodium failure and disturbs the binding process. The swing of E261 is also seen along the Y-axis around 580ns, the moment when the exchange happens (Figure S4). This result shows the swing of E261 plays an important role in this ion-exchange process in cMD4 simulation and in the Na^+ releasing process. aMD simulation is also carried out from the 10ns cMD4 simulation structure for 350ns. The swing of E261, the bridge built between D41 and E261 and the entering of several K^+ ions are all detected and accelerated in the enhanced simulations (no other novel observations and thus shown in Figure S5). The results from aMD1 simulation conforms the interesting conclusions get from cMD4 simulation.

Preprints (www.preprints.org) | NOT PEER-REVIEWED | Posted: 30 August 2018 doi:10.20944/preprints201808.0532.v1

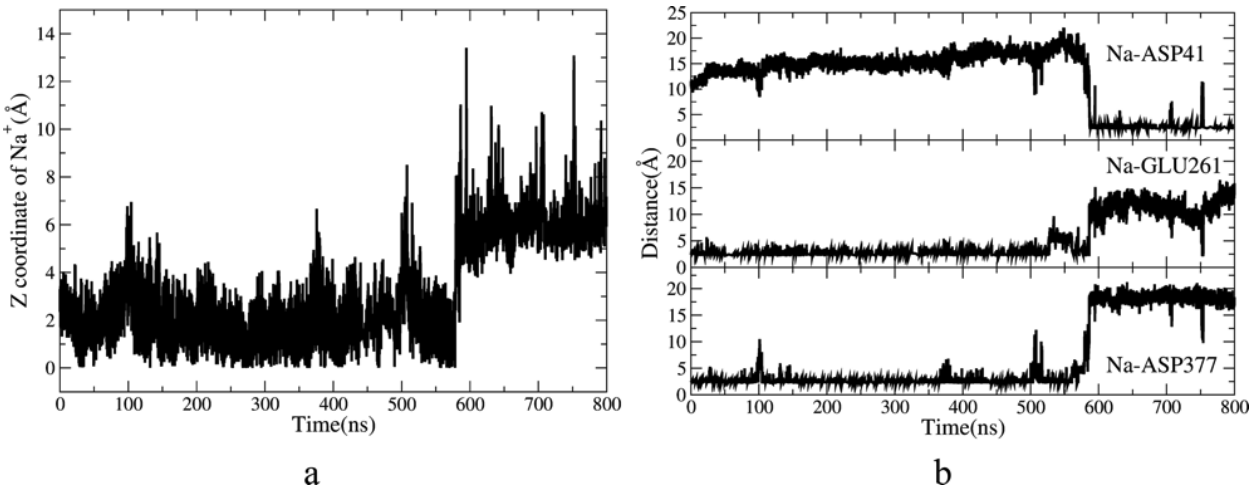

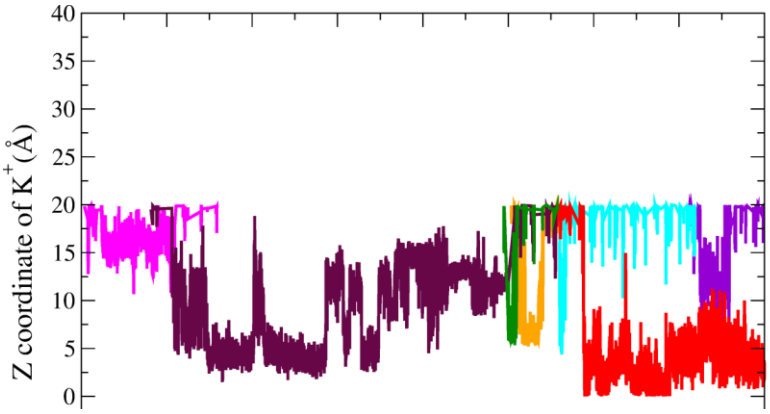

Figure 5. (a) Time evolution of the Z coordinate of Na^+ ion as a function of time in cMD4 simulation. (b) Time evolution of the distance between the bound Na^+ ion and D41/E261/D377.

Time(ns)

Figure 6 Time evolutions of the Z coordinates of the entered K^+ ions into the channel in cMD4 simulation. Each color represents one K^+ ion entering into the channel. There are seven K^+ ions in total drifting into the channel and staying for different simulation time length, and only one finally stays in the binding site (red color).

The analyses of all the simulation results from cMD1 to cMD4 indicate useful and interesting information about the binding process of ions to NorM. The binding of ions involves the right directions of D41, E261 and D377, and the rearrangements of TM1, TM2, TM7, TM8 and TM10.

Proposed binding pathway and binding mechanism of sodium to NorM

The binding site of sodium ion is around the residue of E261 and D377. However, the

 doi:10.20944/preprints201808.0532.v1

dynamics of ions entered into the channel are unknown. The above cMD1 to cMD4 simulations provide lots of insights to the behaviors of ions and key residues of NorM when ions drift into the transport channel. Specifically, in cMD1 simulation, D41 is found to be the first station along the transport pathway of ions, and the wrong direction of E261 leads to the failure of the transport process of ions. These results could be conformed from cMD2 simulation, where E261 positions towards the channel, builds a bridge with D41 and helps ions to be transported into the cation-binding site. Therefore, E261 is defined to be the second station along the transport pathway. In cMD3 simulation, the wrong direction of D41 leads to the collapse of the first station, and disables the entering of ions to the channel. In cMD4 simulation, all the directions of the D41 and E261 are right, and a Na^+-K^+ exchange process happen. That is to say, ions could touch the central cavity and the binding site freely before NorM closes itself. It is reasonable to consider that sodium ion should be able to access the binding site and freely transfer between the three stations D41, E261 and D377 time to time. And at some moment, NorM happens to close itself under the conformational changes due to sodium binding, and the transport cycle begins.

Based on our analyses and other related published results[42, 43] as refers, a working model is proposed to describe the binding pathway of ions, the binding dynamics of key residues along the pathway, and the conformational changes of NorM (shown in Figure 7). As described above, residues D41, E261 and D377 form three significant stations along the pathway of Na^+ ion, and play a critical role in the coordination and transfer of cation to the cation-binding site. In our working model, Na^+ ion is initially loaded from the extracellular side and coordinated directly by the upward of D41 in the outward-facing/substrate-free state of NorM_NG (state a in Figure 7). After that, TM1 and TM7 approach to each other and the E261 turns left and builds a bridge with D41 to coordinate Na^+ ion (state b in Figure 7). Subsequently, E261 returns to the right to locate Na^+ ion in the binding site together with D377. TM7 moves close to TM10, and TM1 and D41 both return to their original sites (state c in Figure 7). Finally, D41 continues to turn to the left and TM2 approaches other TMs to prevent the access of other ions from entering into the binding site and the transport cycle begins (stated in Figure 7). This is the last step before the transporter converts to the inward-facing conformation to uptake a new drug molecule. This working model is hypothetic upon all of the data observed from cMD1 to cMD4 simulations in Table 1, and we expect it will shed some lights on the binding mechanism of ions to cation-binding site.

Preprints (www.preprints.org) | NOT PEER-REVIEWED | Posted: 30 August 2018 doi:10.20944/preprints201808.0532.v1

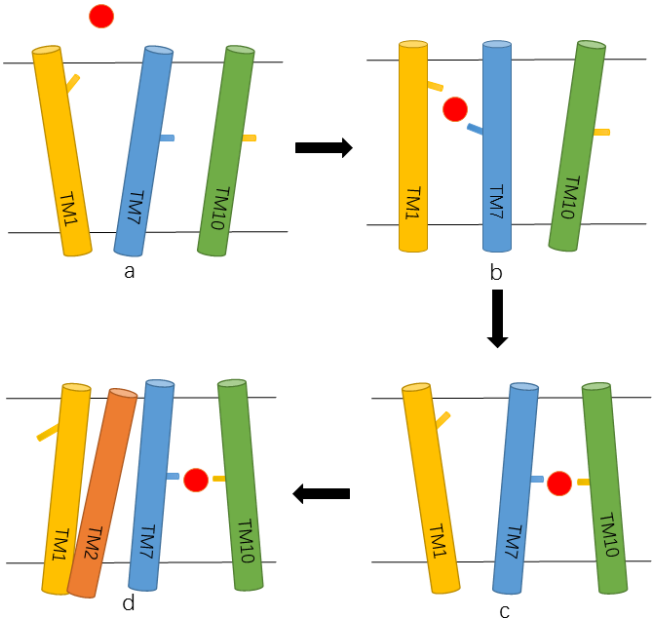

Figure 7. A working model to describe the sodium binding pathway and binding mechanism. Red ball: sodium ion. Line in TM1 is D41. Line in TM7 is E261, and Line in TM10 is D377.

Critical roles of Loop3-4 and Loop9-10 played in substrate-releasing process

As known, long and surface loops always play critical roles in functions of biological molecules[44]. A previous study[14] shows that Loop3-4 and Loop9-10 in NorM are longer and more exposed than other loops, like a 'lid' to cover the central cavity of NorM-NG. It is believed that the flexibility of these two loops probably play a critical role in the extrusion of drug. The three substrates-bound structures of NorM provide solid basis to investigate the relationships between the extrusion of drug and the conformational changes of two loops. Table1 list the details about the four simulations carried on the three different substrates P4P, RHQ, and ETT bound structures in different solvation.

Preprints (www.preprints.org) | NOT PEER-REVIEWED | Posted: 30 August 2018 doi:10.20944/preprints201808.0532.v1

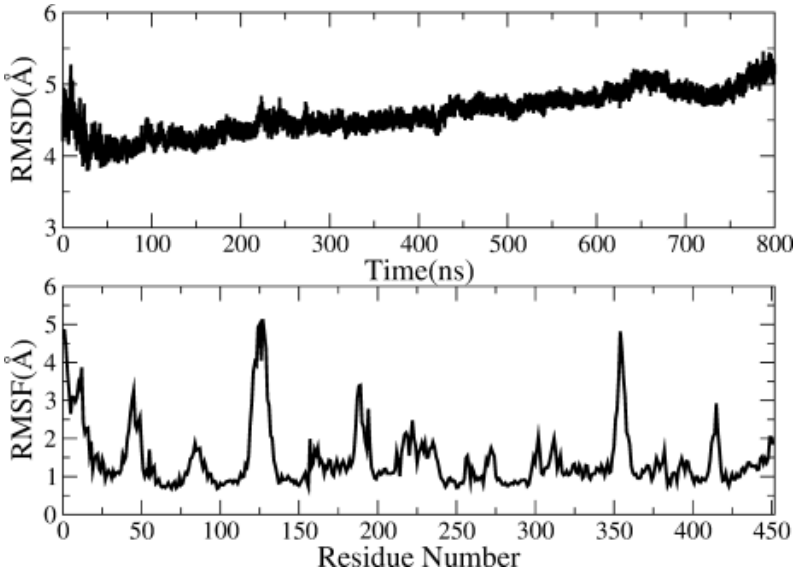

Figure 8 RMSD (top panel) and RMSF (bottom analysis) analysis in cMD5 simulation in Table1

Figure 8 shows the RMSD analysis of NorM during the entire cMD5 simulation time (top panel). It is seen that RMSD reduces to less than 4 Å at 50ns simulation from initial 5 Å, and then rises gradually to around 5.5 Å at the end of 800ns simulation, indicating a large conformational changes of NorM in cMD5 simulation with solvation KCl. RMSF (bottom panel) is used to investigate the specific variances of each residue in NorM to find out the motions leading to the fluctuations of RMSD. The most fluctuate regions in Figure 8 are residues 119-133 and residues 351-359, which precisely and perfectly fit the sequence of Loop3-4 and Loop9-10. The main changes of RMSD come from the long and more exposed loop regions Loop3-4 and Loop9-10.

Then the dynamics of the ligand and these two loops are studied and shown in Figure 9. From the top panel of Figure 9, the Z coordinate of P4P rises heavily from the initial 10 Å to high 22 Å, indicating a large up-move of P4P towards the outside of NorM along its releasing way. The middle panel shows the X coordinate of Loop3-4 goes down from the highest 15Å to about 5Å in 100ns and then stays around 5Å steadily, indicating the twisting of Loop3-4 from the right to the top left. The Z coordinate of Loop9-10 increases from about 21Å to about 30Å, showing the up-move of Loop9-10 along the Z-axis (bottom panel). The detailed structural differences of the flexible Loop3-4 and Loop9-10 are examined before and after MD simulation. Figure S6 shows the simulated final cMD5 snapshot superimposed onto the XRD structure. P4P really goes up after simulation (blue ribbon in left panel of Figure S6), and Loop9-10 rises up (blue color in left panel of Figure S6) in the direction of Z-axis and makes more space for the moving of P4P. The right panel of Figure S6 shows the center of Loop3-4 twists from the right to the top left, consistent with the results got from analysis of coordinates changes in Figure 9. The simultaneous conformational changes of P4P and these two loops reveal an interesting mechanism of transport that the twisting of Loop3-4 and Loop9-10 enlarge the

Preprints (www.preprints.org) | NOT PEER-REVIEWED | Posted: 30 August 2018 doi:10.20944/preprints201808.0532.v1

central cavity and avoid potential steric clashes, finally enable the extrusion of substrate into the extracellular space.

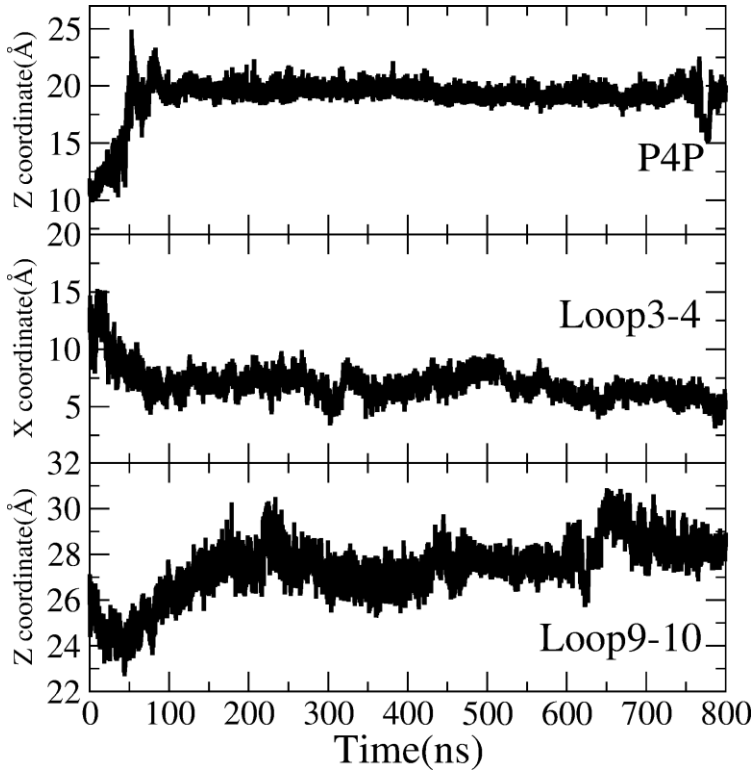

Figure 9 Top panel: time evolutions of Z coordinate of P4P. Middle panel: time evolutions of X coordinate of Loop3-4. Bottom panel: time evolutions of Z coordinate of Loop9-10.

To explicitly investigate the correlations between the motions of Loop3-4 and Loop9-10, Dynamic Cross Correlation Map (DCCM) analysis[45] has been performed on the regions of these two loops and substrate P4P. The DCCM reflects the synchronic correlation between residues intuitively.

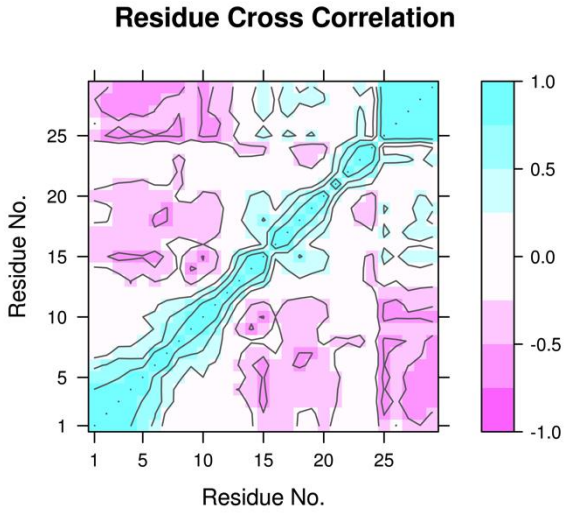

Preprints (www.preprints.org) | NOT PEER-REVIEWED | Posted: 30 August 2018 doi:10.20944/preprints201808.0532.v1

Figure 10 DCCM analysis for P4P-bound-NorM in solvation KCl. Residues 25-26 are for P4P, while residues 1-15 for Loop3-4, and residues 16-24 for Loop 9-10.

Figure 10 shows the DCCM analysis for P4P-bound-NorM in solvation KCl. To make the relations more easily recognized and clarified, four atoms from P4P are used (residues 25-26 in Figure 10), and only name CA used to represents each residue in loops of NorM (residues 1-15 for Loop3-4, residues 16-24 for Loop 9-10). The results show that the motions of P4P have a strong positive correlation with Loop9-10 (cyan color in off-diagonal area), and a strong negative correlation with Loop3-4 (purple color in off-diagonal area). These two opposite correlations exactly make more space for P4P to move and clime up, just like raising the 'lid' on NorM_NG. DCCM analysis clearly shows the motions of P4P strongly correlate with the motions of Loop3-4 and Loop9-10, and opening of the two loops is the preconditions of P4P released from NorM.

NaCl is also used to see the effect of ions on the releasing of substrates. Figure S7 shows the time evolution of Z coordinate of P4P (top panel) and RMSF calculation on NorM_NG for 450 residues during the 800 ns production run in NaCl solution (cMD6 simulation in Table1). The Z coordinate of P4P in cMD6 only sees very little changes (from 1 Å to 2 Å) and remains stable at 12Å throughout the whole simulation. The RMSF analysis shows that neither Loop3-4 (Residue 119-133) nor Loop9-10 (Residue 351-359) fluctuate much as seen in cMD5 simulation with less than 4Å. The substrate P4P surrounded by Na^+ ions does not climb up. These two loops do not move to make more space for P4P, which can be further conformed from DCCM analysis in Figure S8.

The different behaviors of loops and P4P in different solvation show that different ions impact differently on the dynamics of the substrate P4P and may conclude that K^+ ion happens to help the opening of the loops. However, it is only a hypothesis to consider that the motions of biological molecules and its complexes are in an ensemble average, and the opening of these two loops may be just a coincidence. But, the conclusion, definitely conformed, is that Loop3-4 and Loop9-10 play critical roles in the substrate-releasing process, and may be the gate of substrates-releasing that control the leaving of substrates to extracellular side of cell.

Another two MD simulations of the NorM_NG transporter binding with RHQ (cMD7) and ETT (cMD8) in NaCl are performed. RMSF analysis and changes of Z coordinates of substrate analysis are also performed and shown in Figure S9. It is seen that the Z coordinate of RHQ undergoes very small changes. Further, RMSF analysis demonstrates less fluctuating of these Loop3-4 and Loop9-10 (Figure S9a). Figure S9b shows the Z coordinate and the RMSF analysis for ETT from cMD8 simulation. There is no actual extrusion observed in cMD8. RMSF analysis also shows no much fluctuate in motions of Loop3-4 and Loop9-10. These two simulations also conclude that without opening of Loop3-4 and Loop9-10, substrates are not

 doi:10.20944/preprints201808.0532.v1

able to escape into the extracellular side of cell, which can be conformed in the simulation of DCCM analysis for cMD7 (two weak positive correlations detected) and cMD8 (no correlations detected) in Figure S10.

Conclusions

In the present work, molecular dynamics (MD) simulations are performed to study the dynamics of ions binding and the behaviors of the long loops in substrate-releasing process. Three key residues (D41, E261 and D377) are to be found essential in the process of ions entering into the transport channel and reaching the cation-binding site. Based on our analyses, we propose an ion-binding mechanism. D41 is believed to be the first station of ions entering the channel. Without the right direction of D41 towards the channel, the transport of ions is interrupted. Then ions are transferred into the second station E261 with E261 swing into the direction of the channel and building a bridge with D41. Finally, the ions are transported into the cation-binidng site, with E261 swing back to its original crystal position. The rearrangements of TM1, TM7 and TM2 help the transfer of ions between these stations. Further, substrate-bound simulations show two long Loop3-4 and Loop9-10 may control the releasing process. Without the opening of the two loops, substrates can't be able to be pumped into extracellular space. Our findings of the ions dynamics and substrates releasing are on the basis of MD simulations, and hope to shed some lights on the mechanisms under the transport cycle of NorM. More experimental structures are needed to provide evidences for the proposed ions binding mechanisms and critical roles the loops played in the substrate-releasing process.

Acknowledgement

This work was supported by National Key R&D Program of China (Grant no. 2016YFA0501700), National Natural Science Foundation of China (Grant nos. 21433004, 21603144, 91753103), Shanghai Putuo District (Grant 2014-A-02), Innovation Program of Shanghai Municipal Education Commission (201701070005E00020), and NYU Global Seed Grant. We thank the Supercomputer Center of East China Normal University for providing us computer time.

 doi:10.20944/preprints201808.0532.v1

References

1. Lewis, K., *MULTIDRUG-RESISTANCE PUMPS IN BACTERIA - VARIATIONS ON A THEME.* Trends in Biochemical Sciences, 1994. **19**(3): p. 119-123.
2. Nikaido, H., *Multidrug efflux pumps of gram-negative bacteria.* Journal of Bacteriology, 1996. **178**(20): p. 5853-5859.
3. vanVeen, H.W. and W.N. Konings, *Drug efflux proteins in multidrug resistant bacteria.* Biological Chemistry, 1997. **378**(8): p. 769-777.
4. Lu, M., *Structures of multidrug and toxic compound extrusion transporters and their mechanistic implications.* Channels, 2016. **10**(2): p. 88-100.
5. Kuroda, T. and T. Tsuchiya, *Multidrug efflux transporters in the MATE family.* Biochimica Et Biophysica Acta-Proteins and Proteomics, 2009. **1794**(5): p. 763-768.
6. Higgins, C.F., *Multiple molecular mechanisms for multidrug resistance transporters.* Nature, 2007. **446**(7137): p. 749-757.
7. Omote, H., et al., *The MATE proteins as fundamental transporters of metabolic and xenobiotic organic cations.* Trends in Pharmacological Sciences, 2006. **27**(11): p. 587-593.
8. Masuda, S., et al., *Identification and functional characterization of a new human kidney-specific H+/organic cation antiporter, kidney-specific multidrug and toxin extrusion 2.* Journal of the American Society of Nephrology, 2006. **17**(8): p. 2127-2135.
9. Yonezawa, A. and K. Inui, *Importance of the multidrug and toxin extrusion MATE/SLC47A family to pharmacokinetics, pharmacodynamics/toxicodynamics and pharmacogenomics.* British Journal of Pharmacology, 2011. **164**(7): p. 1817-1825.
10. Motohashi, H. and K. Inui, *Multidrug and toxin extrusion family SLC47: Physiological, pharmacokinetic and toxicokinetic importance of MATE1 and MATE2-K.* Molecular Aspects of Medicine, 2013. **34**(2-3): p. 661-668.
11. Staud, F., et al., *Multidrug and toxin extrusion proteins (MATE/SLC47); role in pharmacokinetics.* International Journal of Biochemistry & Cell Biology, 2013. **45**(9): p. 2007-2011.
12. He, X.A., et al., *Structure of a cation-bound multidrug and toxic compound extrusion transporter.* Nature, 2010. **467**(7318): p. 991-U139.
13. Morita, Y., et al., *NorM of Vibrio parahaemolyticus is an Na+-driven multidrug efflux pump.* Journal of Bacteriology, 2000. **182**(23): p. 6694-6697.
14. Lu, M., et al., *Structures of a Na+-coupled, substrate-bound MATE multidrug transporter.* Proceedings of the National Academy of Sciences of the United States of America, 2013. **110**(6): p. 2099-2104.
15. Song, J.N., C.G. Ji, and J.Z.H. Zhang, *Insights on Na+ binding and conformational dynamics in multidrug and toxic compound extrusion transporter NorM.* Proteins-Structure Function and Bioinformatics, 2014. **82**(2): p. 240-249.
16. Brooks, B.R., et al., *CHARMM: The Biomolecular Simulation Program.* Journal of Computational Chemistry, 2009. **30**(10): p. 1545-1614.
17. Brooks, B.R., et al., *CHARMM - A PROGRAM FOR MACROMOLECULAR ENERGY, MINIMIZATION, AND DYNAMICS CALCULATIONS.* Journal of Computational Chemistry, 1983. **4**(2): p. 187-217.
18. Jo, S., et al., *Software news and updates - CHARNIM-GUI: A web-based grraphical user interface for CHARMM.* Journal of Computational Chemistry, 2008. **29**(11): p. 1859-1865.

19. Lee, J., et al., *CHARMM-GUI Input Generator for NAMD, GROMACS, AMBER, OpenMM, and CHARMM/OpenMM Simulations Using the CHARMM36 Additive Force Field.* Journal of Chemical Theory and Computation, 2016. **12**(1): p. 405-413.
20. Feller, S.E., *Molecular dynamics simulations of lipid bilayers.* Current Opinion in Colloid & Interface Science, 2000. **5**(3-4): p. 217-223.
21. Wang, Y., et al., *Enhanced Lipid Diffusion and Mixing in Accelerated Molecular Dynamics.* Journal of Chemical Theory and Computation, 2011. **7**(10): p. 3199-3207.
22. Jorgensen, W.L., et al., *COMPARISON OF SIMPLE POTENTIAL FUNCTIONS FOR SIMULATING LIQUID WATER.* Journal of Chemical Physics, 1983. **79**(2): p. 926-935.
23. Bour, P. and T.A. Keiderling, *AB-INITIO SIMULATIONS OF THE VIBRATIONAL CIRCULAR-DICHROISM OF COUPLED PEPTIDES.* Journal of the American Chemical Society, 1993. **115**(21): p. 9602-9607.
24. Wang, J.M., et al., *Development and testing of a general amber force field.* Journal of Computational Chemistry, 2004. **25**(9): p. 1157-1174.
25. Case, D.A., et al., *The Amber biomolecular simulation programs.* Journal of Computational Chemistry, 2005. **26**(16): p. 1668-1688.
26. Salomon-Ferrer, R., D.A. Case, and R.C. Walker, *An overview of the Amber biomolecular simulation package.* Wiley Interdisciplinary Reviews-Computational Molecular Science, 2013. **3**(2): p. 198-210.
27. Pearlman, D.A., et al., *AMBER, A PACKAGE OF COMPUTER-PROGRAMS FOR APPLYING MOLECULAR MECHANICS, NORMAL-MODE ANALYSIS, MOLECULAR-DYNAMICS AND FREE-ENERGY CALCULATIONS TO SIMULATE THE STRUCTURAL AND ENERGETIC PROPERTIES OF MOLECULES.* Computer Physics Communications, 1995. **91**(1-3): p. 1-41.
28. Darden, T., D. York, and L. Pedersen, *PARTICLE MESH EWALD - AN N.LOG(N) METHOD FOR EWALD SUMS IN LARGE SYSTEMS.* Journal of Chemical Physics, 1993. **98**(12): p. 10089-10092.
29. Essmann, U., et al., *A SMOOTH PARTICLE MESH EWALD METHOD.* Journal of Chemical Physics, 1995. **103**(19): p. 8577-8593.
30. Ryckaert, J.P., G. Ciccotti, and H.J.C. Berendsen, *NUMERICAL-INTEGRATION OF CARTESIAN EQUATIONS OF MOTION OF A SYSTEM WITH CONSTRAINTS - MOLECULAR-DYNAMICS OF N-ALKANES.* Journal of Computational Physics, 1977. **23**(3): p. 327-341.
31. Pastor, R.W., B.R. Brooks, and A. Szabo, *AN ANALYSIS OF THE ACCURACY OF LANGEVIN AND MOLECULAR-DYNAMICS ALGORITHMS.* Molecular Physics, 1988. **65**(6): p. 1409-1419.
32. Voter, A.F., *Hyperdynamics: Accelerated molecular dynamics of infrequent events.* Physical Review Letters, 1997. **78**(20): p. 3908-3911.
33. Hamelberg, D., J. Mongan, and J.A. McCammon, *Accelerated molecular dynamics: A promising and efficient simulation method for biomolecules.* Journal of Chemical Physics, 2004. **120**(24): p. 11919-11929.
34. De Oliveira, C.A.F., D. Hamelberg, and J.A. McCammon, *Estimating kinetic rates from accelerated molecular dynamics simulations: Alanine dipeptide in explicit solvent as a case study.* Journal of Chemical Physics, 2007. **127**(17).
35. Hamelberg, D., C.A.F. de Oliveira, and J.A. McCammon, *Sampling of slow diffusive*

conformational transitions with accelerated molecular dynamics. Journal of Chemical Physics, 2007. **127**(15).

36. de Oliveira, C.A.F., D. Hamelberg, and J.A. McCammon, *Coupling accelerated molecular dynamics methods with thermodynamic integration simulations.* Journal of Chemical Theory and Computation, 2008. **4**(9): p. 1516-1525.
37. Bucher, D., et al., *Accessing a Hidden Conformation of the Maltose Binding Protein Using Accelerated Molecular Dynamics.* Plos Computational Biology, 2011. **7**(4).
38. Markwick, P.R.L. and J.A. McCammon, *Studying functional dynamics in bio-molecules using accelerated molecular dynamics.* Physical Chemistry Chemical Physics, 2011. **13**(45): p. 20053-20065.
39. Wang, Y., et al., *Implementation of Accelerated Molecular Dynamics in NAMD.* Computational Science and Discovery, 2011. **4**(1): p. 015002 (10 pp.)-015002 (10 pp.).
40. Sinko, W., et al., *Protecting High Energy Barriers: A New Equation to Regulate Boost Energy in Accelerated Molecular Dynamics Simulations.* Journal of Chemical Theory and Computation, 2012. **8**(1): p. 17-23.
41. Tikhonova, I.G., et al., *Simulations of Biased Agonists in the beta(2) Adrenergic Receptor with Accelerated Molecular Dynamics.* Biochemistry, 2013. **52**(33): p. 5593-5603.
42. Vanni, S., et al., *Ion Binding and Internal Hydration in the Multidrug Resistance Secondary Active Transporter NorM Investigated by Molecular Dynamics Simulations.* Biochemistry, 2012. **51**(6): p. 1281-1287.
43. Leung, Y.M., et al., *The NorM MATE Transporter from N-gonorrhoeae: Insights into Drug and Ion Binding from Atomistic Molecular Dynamics Simulations.* Biophysical Journal, 2014. **107**(2): p. 460-468.
44. Song, J.N., et al., *Functional Loop Dynamics of the Streptavidin-Biotin Complex.* Scientific Reports, 2015. **5**.
45. Bowerman, S. and J. Wereszczynski, *Detecting Allosteric Networks Using Molecular Dynamics Simulation*, in *Computational Approaches for Studying Enzyme Mechanism, Pt B*, G.A. Voth, Editor. 2016, Elsevier Academic Press Inc: San Diego. p. 429-447.

Acknowledgements

This work was supported by National Key R&D Program of China (Grant no. 2016YFA0501700), National Natural Science Foundation of China (Grant nos. 21433004, 21603144, 91753103), Shanghai Sailing Program (Grant no. 2016YF1408400), Shanghai Putuo District (Grant 2014-A-02), Innovation Program of Shanghai Municipal Education Commission (201701070005E00020), and NYU Global Seed Grant. We thank the Supercomputer Center of East China Normal University for providing us computer time.

Author Contributions

J.D performed computation with the assistance of G.F.D, C.G.J interpreted data, J.N.S and J.Z.H.Z designed and prepared manuscript. All authors have read and approved the submission of the manuscript.

Additional Information

Supplementary information accompanies this paper at https://doi.org/xxxx

Competing Interests: The authors declare no competing interests.

Preprints (www.preprints.org) | NOT PEER-REVIEWED | Posted: 30 August 2018 doi:10.20944/preprints201808.0532.v1

Figure Captions

Figure 1

The dynamics of Na^+ and E261 in Apo-NorM simulation in solvation NaCl Top panel: the changes of distance between the entered Na^+ ion and D41 as a function of time. Middle panel: the changes of Z coordinate of COO- of E261 as a function of time. Pink color: the directions of COO^- in XRD structure, bule color: the direction of COO^- in the final MD structure. Bottom panel: The distributions of Z coordinates of COO^- of E261 during 800 ns simulation.

Figure 3

Time evolutions of the distance between the two entered K^+ ion and D41/E261

Figure 3

Time evolutions of the Y coordinates of COO^- group of D41 (black line) Red line: the Y coordinates of COO^- group of D41 in XRD structure. Pink color: the directions of COO^- in XRD structure, Light bule color: the direction of COO^- in the final MD structure.

Figure 4

The final MD structure (light blue color) of NorM in cMD3 is superimposed to the initial XRD structure (pink color), with TM2 enlarged in the bottom left of this figure.

Figure 5

(a) Time evolution of the Z coordinate of Na^+ ion as a function of time in cMD4 simulation. (b) Time evolution of the distance between the bound Na^+ ion and D41/E261/D377.

Figure 6

time evolutions of the Z coordinates of the entered K^+ ions into the channel in cMD4 simulation. Each color represents one K^+ ion entering into the channel. There are seven K^+ ions in total drifting into the channel and staying for different simulation time length, and only one finally stays in the binding site (red color).

Figure 7

A working model to describe the sodium binding pathway and binding mechanism Red ball: sodium ion. Line in TM1 is D41. Line in TM7 is E261, and Line in TM10 is D377.

Figure 8

RMSD (top panel) and RMSF (bottom analysis) analysis in cMD5 simulation in Table1

Figure 9

Top panel: time evolutions of Z coordinate of P4P. Middle panel: time evolutions of X coordinate of Loop3-4. Bottom panel: time evolutions of Z coordinate of Loop9-10.

Figure 10

DCCM analysis for P4P-bound-NorM in solvation KCl. Residues 25-26 are for P4P, while residues 1-15 for Loop3-4, residues 16-24 for Loop 9-10.